ELSEVIER

NeuroImage

www.elsevier.com/locate/ynimg
NeuroImage 29 (2005) 99 – 105

Neuroanatomical differences between mouse strains as shown by high-resolution 3D MRI

X. Josette Chen,[a,*] Natasa Kovacevic,[a] Nancy J. Lobaugh,[b] John G. Sled,[a] R. Mark Henkelman,[a] and Jeffrey T. Henderson[c]

[a]*Mouse Imaging Centre, Hospital for Sick Children, Department of Medical Biophysics, 555 University Avenue, Toronto, Ontario, Canada M5G 1X8*
[b]*Imaging Research Cognitive Neurology, Sunnybrook and Women's College Health Sciences Centre, University of Toronto, Toronto, Canada*
[c]*Department of Pharmaceutical Sciences, Leslie Dan Faculty of Pharmacy, University of Toronto, Toronto, Canada*

Received 24 January 2005; revised 29 June 2005; accepted 5 July 2005
Available online 9 August 2005

The search for new mouse models of human disease requires a sensitive metric to make three-dimensional (3D) anatomical comparisons in a rapid and quantifiable manner. This is especially true in the brain, where changes in complex shapes such as the hippocampus and ventricles are difficult to assess with 2D histology. Here, we report that the 3D neuroanatomy of three strains of mice (129S1/SvImJ, C57/Bl6, and CD1) is significantly different from one another. Using image co-registration, we 'morphed' together nine brains of each strain scanned by magnetic resonance imaging at (60 μm)^3 resolution to synthesize an average image. We applied three methods of comparison. First, we used visual inspection and graphically examined the standard deviation of the variability in each strain. Second, we annotated 42 neural structures and compared their volumes across the strains. Third, we assessed significant local deviations in volume and displacement between the two inbred strains, independent of prior anatomical knowledge.
© 2005 Elsevier Inc. All rights reserved.

Introduction

The analysis and processing of medical images, especially human brain images, for the purpose of determining quantitative measures of function and anatomy is a rich and evolved field. With growing interest in the genetic basis of neuroanatomy, such tools have become even more valuable. Experiments performed in mice frequently use controlled genetic backgrounds and researchers would like to be able to identify mutant outliers which differ only slightly from controls. Properly applied image processing tools can recognize such differences that may not be immediately apparent and can do so in a rapid and reproducible fashion.

Before any measurements can be made on neural mutants, however, the boundaries of what constitutes a wildtype central nervous system (CNS) must be established. In other words, we must determine the level of variability within a control population for a given experimental measure. In the case of anatomy, comparisons can be difficult because morphology is inherently 3D. Morphological differences between strains have been studied at the histologic level (Wahlsten et al., 2003; Tabibnia et al., 1999). However, histologic comparisons are, by necessity, two dimensional and section-to-section alignment is affected by the process of slicing.

We have developed techniques in which 3D, non-destructive, high-resolution magnetic resonance (MR) imaging is used in conjunction with automated image processing tools to assess commonalities and differences in the whole mouse brain and its structures (Kovacevic et al., 2005). Mouse brains are excised and MR imaged at 60 μm resolution isotropic. The brains are first linearly registered to remove any differences in overall size and shape—a global normalization. Then, non-linear registration is applied to these globally normalized images to bring the individual brains into an unbiased average image. The transformation information is expressed as the displacement of each point in the image: a deformation field. In this study, we have applied these techniques to three different strains of mice using nine brains for each strain: 129S1/SvImJ (129Sv), C57/Bl6 (C57), and the outbred line CD1. We have chosen these inbred strains as they are commonly used in knockout and random mutagenesis studies and CD1 as it is one of the most widely utilized outbred strains. We developed three independent methods to detect differences between the groups of mice. First, we graphically and quantitatively mapped out the spatial variation of the deformation fields within each strain and between strains. Second, we compared segmented volumes of specific brain structures in the three strains. Finally, we derived two measures from the deformation fields: local volume changes and positional shifts between the two inbred strains. To assess the differences, we used multivariate statistical tools to make voxel-wise comparisons.

* Corresponding author. Fax: +1 416 813 2208.
E-mail address: josette@sickkids.ca (X.J. Chen).
Available online on ScienceDirect (www.sciencedirect.com).

1053-8119/$ - see front matter © 2005 Elsevier Inc. All rights reserved.
doi:10.1016/j.neuroimage.2005.07.008

Methods

Brain preparation

All procedures performed conform to University of Toronto and National Institutes of Health guidelines on animal care. Eight-week-old male outbred CD1 (Charles River, Wilmington, MA) mice, inbred C57/Bl6 (Jackson Laboratory, Bar Harbor, ME) mice, and inbred 129S1/SvImJ mice (Jackson Laboratory) were acclimated for a period of 3 days. Animals were then anesthetized with an overdose of Avertin (2.5%) via intraperitoneal injection. Following lack of deep tendon responses, the thoracic cavity was opened and animals perfused through the left ventricle with 10 cm^3 of 0.1 M phosphate buffer (pH 7.4) 0.9% NaCl (PBS), followed by 4% formaldehyde in PBS. Solutions were infused at room temperature (25°C). Following perfusion, the heads were removed and allowed to postfix in solution at room temperature for an additional 60 min, at which time the cranium was opened and the brain removed in its entirety. Brains were then postfixed for an additional 24 h in a 4% paraformaldehyde in PBS at room temperature.

Magnetic resonance imaging

A 7.0-T, 40-cm bore magnet (Magnex Scientific, Oxford, UK) with a 29-cm inner bore diameter gradient set (Tesla Engineering Ltd., Storrington, Sussex, UK) and connected to a Unity^{INOVA} console (Varian Instruments, Palo Alto, CA) was used to acquire anatomical images of excised brains. Prior to imaging, the brains were removed from the fixative and placed into glass tubes filled with a proton-free susceptibility-matching fluid (Fluorinert FC-77, 3M Corp., St. Paul, MN). We used four custom-built, 12-mm over-wound uniform solenoid coils (Idziak and Haeberlen, 1982) with four parallel receivers to image four brains in parallel. The parameters used in the brain scans were optimized for gray/white matter contrast: T2-weighted, 3D spin-echo sequence, with TR/TE = 1600/35 ms, single average, field-of-view = 12 × 12 × 24 mm and matrix size = 200 × 200 × 400 giving an image with (60 μm)^3 isotropic voxels. The total imaging time was 18.5 h.

Image registration

We used a previously developed image registration technique for deriving unbiased group averages (Kovacevic et al., 2004). Briefly, given a group of n brain images, the algorithm initially performs normalization of all brains with respect to global orientation, size, shape, and MR intensity. This initial normalization step relies on affine transformations only and is assumed to remove non-significant anatomical differences. Next, the algorithm proceeds with group-wise non-linear registration, followed by geometric centering to produce two outputs: (1) a consensus average brain anatomy and (2) a set of n deformation fields which encode anatomical differences between the group average and individual globally normalized brains. For each anatomical landmark (voxel) in the group average, the n anatomically homologous locations within globally normalized individual brains represent the spatial variability of the landmark across the group. Details of the algorithm and validation can be found in Kovacevic et al. (2004). We applied this algorithm several times. Firstly, in order to factor out non-significant differences, regardless of mouse strain, we globally normalized all 27 brains to obtain a grand average (n = 27). We then produced three strain-specific averages (n = 9 for each strain). For the comparison of the two inbred strains, we also produced their collective average (n = 18). All these average brain images were formed by averaging the signal intensities of the individual warped images.

CNS structure labeling

The average brain based on all 27 brains was annotated by registering with a previously annotated 129Sv brain atlas (Kovacevic et al., 2005). This annotation was then transformed along the deformation fields to the 27 individual globally normalized brains. In this way, all 27 individual brains were labeled. The software package Amira (TGS Inc., San Diego, CA) was used for 3D visualization to evaluate the accuracy of the automated segmentation of each of the 27 input brain images. Where needed, minor corrections were made to the individual segmentations.

Deformation fields

In a standard image registration framework, anatomical differences between two brains are encoded by a deformation field F, such that for each location x in the first brain, $F(x)$ represents the vector to

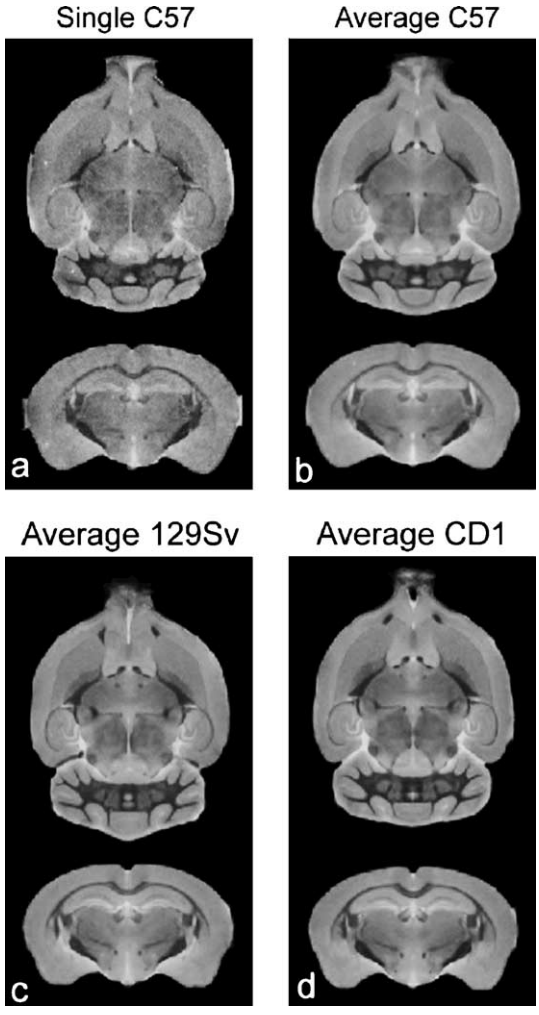

Fig. 1. Horizontal and coronal views of an individual brain and average images. (a) A single C57 brain, (b) the average C57 brain, (c) the average 129Sv brain, and (d) the average CD1 brain. All images are shown with the same contrast.

the anatomically homologous location in the second brain, as estimated by the registration algorithm. We used two main measures derived from deformation fields: deformation magnitude as a measure of positional distance within a fixed coordinate system and Jacobian of the displacement field as a measure of local volumetric change. These scalar measures provided summary measures of the combination of shape and size and location differences across the strains, simplifying the statistical analysis and interpretation of voxel-wise difference across strains. They also avoid the unstable estimation of multivariate statistics of full vector deformation fields.

For the purpose of estimating group-wise variability, we used a previously introduced measure of the standard deviation of the deformation magnitudes SDDM:

$$\mathrm{SDDM}(x) = \sqrt{\frac{1}{n-1}\sum_{k}\|F_k(x)\|^2}$$

for every voxel x in the average and $F_1 - F_n$ are deformation fields from the average onto each of the n individuals. By calculating the mean over all brain voxels x, we produce a single number, mean SDDM, as a rough estimate of the overall variability for a given group.

Partial least squares (PLS)

Anatomical differences between mouse strains can be visualized using magnitudes of the deformation fields from each mouse strain into the average image. However, these maps do not, by themselves, indicate which aspects of the deformation fields most strongly distinguish the mouse strains. A general feature of neuroimaging data is that it is multidimensional, which poses problems for traditional statistical analyses. These problems have been partially overcome by the incorporation of random-field theory for univariate voxel-based analyses (Friston et al., 1996, Worsley et al., 2004). A complementary approach is to highlight the multivariate nature of the data sets by using a combination of multivariate and distribution-free approaches, such as PLS. PLS has been used to analyze functional neuroimaging data to identify areas of activity commonly differentiating experimental conditions. For the present work, we sought to identify, across the full deformation data set, those regions most strongly distinguishing the two inbred strains. Two data sets were created from the deformation fields, reflecting voxel-wise magnitudes of volumetric and displacement differences between the inbred strains. Volumetric comparisons were derived using the Jacobian, which provides a measure of expansion or contraction (Chung et al., 2001). For displacements, we used scalar distances along the direction connecting the homologous voxels of the strain average images as introduced by Lancaster et al. (2003). Since each of these metrics is scalar, they were analyzed with a one-dimensional PLS mean-centered approach as described by McIntosh and Lobaugh (2004).

Two non-parametric methods were used to test the significance and reliability of the findings. Permutation tests (n = 500) were used to test the significance of the latent variables. The differences between the C57 and 129Sv strains for the Jacobians were significant at P = 0.002, and for the displacement data at P = 0.004. Bootstrap resampling (n = 200) was used to calculate the standard error of the voxel saliences in the singular images. The ratio of the salience to the bootstrap standard error is roughly a z score (assuming normality in the bootstrap distribution). We set this bootstrap ratio threshold to five for the Jacobian data (top 4% of voxels) and 10 (top 8% of voxels) for the displacement data. PLS has been implemented as MATLAB code (The MathWorks, Natick, MA) and can be found at http://www.rotman-baycrest.on.ca:8080.

Results

The process of non-linearly aligning and averaging together a number of genetically identical brains generally yields a much

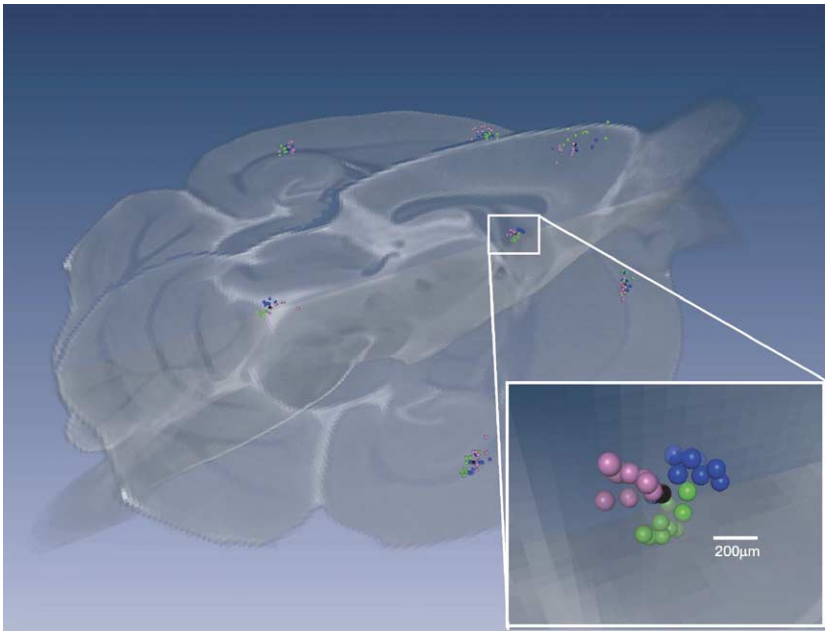

Fig. 2. Several anatomical landmarks and their spatial distribution across all 27 brains. For each landmark, the large black ball represents a location in the grand average, while corresponding 129Sv, C57, and CD1 locations are represented by pink, green, and blue balls, respectively. The grayscale image is the average image of the 27 brains. The inset image is a zoom-in of the indicated cluster.

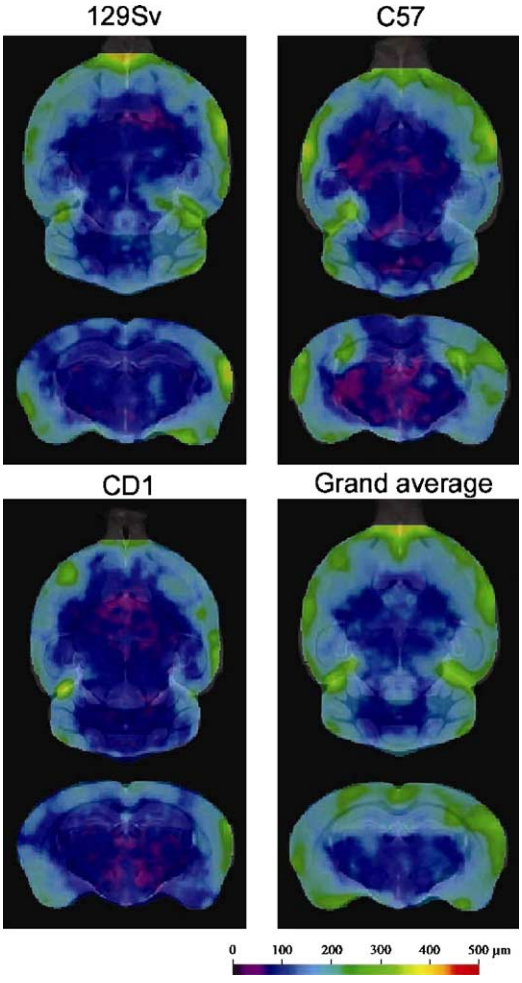

Fig. 3. Horizontal (top) and coronal (bottom) views of the standard deviation of the deformation magnitude images (SDDM) overlaid on the corresponding grayscale images. The average SDDM was 149 ± 55 μm, 150 ± 63 μm, 129 ± 48 μm, and 181 ± 63 μm, for the 129Sv average, C57 average, CD1 average, and the grand average.

sharper image, as shown in the C57 strain in Fig. 1b as compared with Fig. 1a. This "sharpness" has been shown to be a reliable measure of the accuracy of registration (Robbins et al., 2004). This suggests that the primary neural structures are very similar in genetically identical individuals at a resolution of $(60\ \mu m)^3$. However, structures on the order of the imaging resolution, such as small blood vessels and arteries, tend to be blurred out in the average image, suggesting that these structures are not under tight genetic control. The average brains from the 129Sv and CD1 mice are shown in Figs. 1c and d, respectively. Detailed visual inspection reveals many subtle anatomical differences among the strains, e.g., the width of the corpus callosum (coronal section) and the complexity of the myelinated tracts in the cerebellum (horizontal sections).

A further means of comparing differences across strains is through direct visualization of the displacement fields. The grand average of all 27 brains is shown in two orthogonal planes in Fig. 2. The black balls correspond to arbitrary voxels in the grand average. The homologous voxels of the individual 129Sv are represented by pink balls, C57 by green, and CD1 by blue. As expected, voxels from each individual strain tend to cluster together and it is trivial to observe that the inter-strain variability is greater than the intra-strain variability.

More quantitative measures of the variability can be derived from the deformation fields obtained in the creation of the average brains. Fig. 3 shows views of the SDDM from the three strains and the grand average of all 27 brains on a spectral color scale overlaid on the grayscale anatomical image. The areas of high variability (green and yellow) are on the outer surface of the brain and at the point of flexure between the cortex and the cerebellum. This is to be expected for excised brain samples due to handling procedures. In future studies, we recommend and we will implement leaving the brain in the skull to minimize surface deformations as described by Tyszka et al. (submitted for publication). The interior of all the brains shows much less variability. As expected, the grand average of all 27 brains shows the greatest variability and has the smallest number of voxels with less than 100 μm displacement. This way of rendering the variability also reveals more localized spatial information. For instance, in all strains, the more proximal arbor vita exhibits lower variability than the outer cerebellar folia.

By averaging over all the voxels for each average brain, we found the mean SDDM (± its standard deviation) was 149 ± 55 μm, 150 ± 63 μm, and 129 ± 48 μm for the 129Sv, C57, and CD1, respectively; whereas the average SDDM for all 27 brains was larger at 181 ± 63 μm. This result quantifies the visual observation

Table 1
The normalized average volumes (% of total brain volume ± % standard deviation) of selected structures in the three strains

Region of interest	129S1/SvImJ (mean ± σ %)	C57/Bl6 (mean ± σ %)	CD1 (mean ± σ %)
3rd and 4th ventricle cerebral aqueduct	0.58 ± 0.05	0.60 ± 0.04	0.53 ± 0.04
Amygdaloid region ventral	1.65 ± 0.14	1.64 ± 0.13	1.56 ± 0.06
Anterior commissure pars anterior	0.13 ± 0.008	0.13 ± 0.008	0.13 ± 0.005
Anterior commissure pars posterior	0.056 ± 0.006	0.053 ± 0.003	0.060 ± 0.003
Arbor vita	2.62 ± 0.12	2.18 ± 0.09	2.42 ± 0.10
Cerebellum gray matter	11.70 ± 0.49	10.35 ± 0.26	10.91 ± 0.26
Corpus callosum	3.67 ± 0.11	3.71 ± 0.05	3.72 ± 0.20
Cortex	31.5 ± 0.8	34.4 ± 0.5	31.4 ± 0.7
Dentate gyrus	0.41 ± 0.04	0.38 ± 0.02	0.36 ± 0.02
Facial nerve	0.059 ± 0.003	0.056 ± 0.003	0.060 ± 0.005
Fimbria	0.63 ± 0.02	0.63 ± 0.02	0.67 ± 0.04
Fornix	0.095 ± 0.006	0.096 ± 0.003	0.090 ± 0.005
Habenulo peduncular tract	0.042 ± 0.003	0.040 ± 0.003	0.050 ± 0.003
Hippocampus gray matter	5.76 ± 0.18	5.65 ± 0.10	5.61 ± 0.16
Internal capsule	0.60 ± 0.02	0.55 ± 0.01	0.60 ± 0.04
Lateral ventricles	0.37 ± 0.02	0.64 ± 0.10	0.40 ± 0.02
Mammilo-thalamic tract	0.053 ± 0.003	0.045 ± 0.003	0.054 ± 0.005
Medial septum	0.33 ± 0.034	0.31 ± 0.016	0.32 ± 0.019
Optic tract	0.22 ± 0.01	0.19 ± 0.01	0.21 ± 0.01
Posterior commissure	0.020 ± 0.001	0.021 ± 0.003	0.020 ± 0.003
Pre and para subiculum	0.60 ± 0.07	0.65 ± 0.08	0.58 ± 0.05
Stria terminalis	0.048 ± 0.003	0.05 ± 0.005	0.05 ± 0.003
Striatum	5.06 ± 0.15	5.29 ± 0.12	5.50 ± 0.23

The total brain volumes for the three strains were 357 ± 8 mm^3, 375 ± 4 mm^3, and 367 ± 4 mm^3 for the 129Sv, C57, and CD1, respectively.

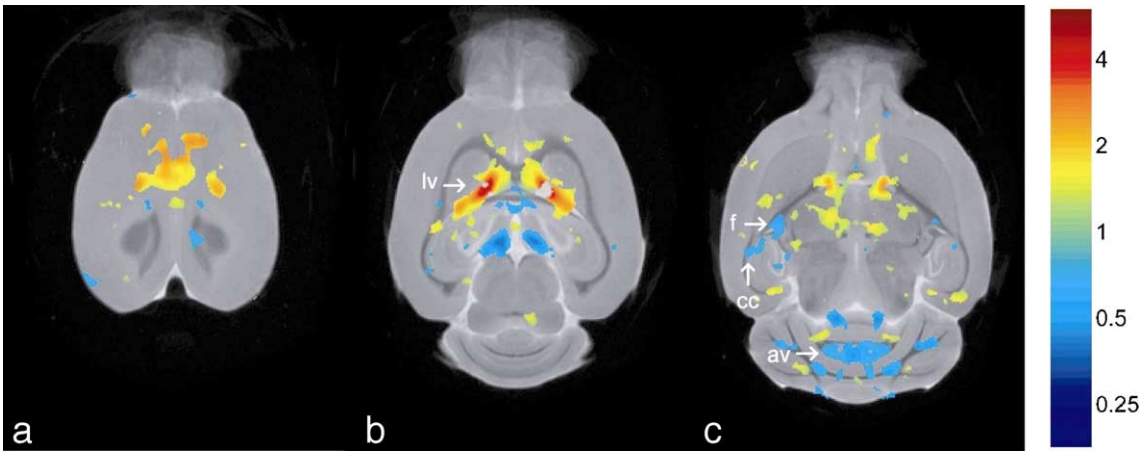

Fig. 4. Selected horizontal views showing statistically significant local volume expansions (yellow/red) and contractions (blue) in the C57 strain compared to the 129Sv strain combined with expansion f the anterior corpus callosum. The color scale is a logarithmic representation with colors greater than 1.0 showing expansion and less than 1.0 showing contraction. For these particular slices, we show (a) local expansion in the rostral aspect of the cortex, (b) expansion of the lateral ventricles (lv), and (c) contraction of the fimbria (f), corpus callosum (cc), and the proximal arbor vita (av).

in both Figs. 2 and 3. The equivalent efficacy of the registration algorithm for each of the three strains of mice can be appreciated from these results. If the registration was ineffective for one strain, it would have a smaller average SDDM, a dissimilar SDDM map in Fig. 3 and a more blurry average image in Fig. 1. None of these appear to be the case, implying that the registration performs equivalently for each strain.

The overall size and shape of the brains from the three strains appear different as do some of the interior structures. To quantitatively identify these differences, we used the manual segmentation of 42 manually segmented structures in the 129Sv average brain presented in Kovacevic et al., 2005. From this one average brain, we used our computed deformation fields to transform and customize these labels to each of the 27 individual brains. We then calculated the volumes for each structure by counting the numbers of voxels within each label. A listing of selected structures and their corresponding normalized volumes in the three strains are shown in Table 1 (see http://www.mouseimaging.ca/var_brain_atlas.html for all of the segmented structures).

The volumetric analysis of brain structures was based upon known anatomical definitions for the manual labeling. However, by deriving two independent measures from the deformation fields, we were able to compare local volume changes and shifts on a voxel-wise basis between the two inbred strains without using a priori structural information using PLS. The global analysis showed for both measures that there were statistically significant differences between the two strains.

Fig. 4 shows the results of the PLS analysis for the Jacobian data. The horizontal views highlight voxels where the local expansions and contractions were consistent across individuals. Areas in yellow and red indicate regions that expanded in the C57 strain compared to the 129Sv strain and areas in blue are contracted in the C57 strain.

In Fig. 4a, we see that the rostral aspect of the cortex is expanded in C57 compared to 129Sv. Verifying what was seen in the segmentation analysis, the lateral ventricles of the C57 are expanded (Fig. 4b) and the arbor vita are contracted (Fig. 4c). Fig. 4c also shows a mild contraction in the vicinity of the fimbria that is stable across individuals. A finding that could not have been discovered in the volumetric analysis was that both expansion and contraction defined the differences between these two strains. From Table 1, we saw that, on the whole, the C57 corpus callosum was larger than 129Sv. However, parts of the corpus callosum (vertical arrow, Fig. 4c) were actually smaller in C57 than in the 129Sv. In contrast to this local reduction, the corpus callosum is expanded near the genu (Fig. 4c, horizontal arrow). Examination across the entire volume verified that there were more local expansions of the corpus callosum than contractions.

The second PLS analysis focused on the magnitude of the displacement between the two strains (Lancaster et al., 2003). Fig. 5 shows regions where the difference in directional distance between the two strains was stable. The color scale indicates how far the C57 strain was displaced in relation to the 129Sv strain in micrometers. We see that bilateral hippocampus and bilateral anterior corpus callosum have shifted by as much as 400 μm between the two strains.

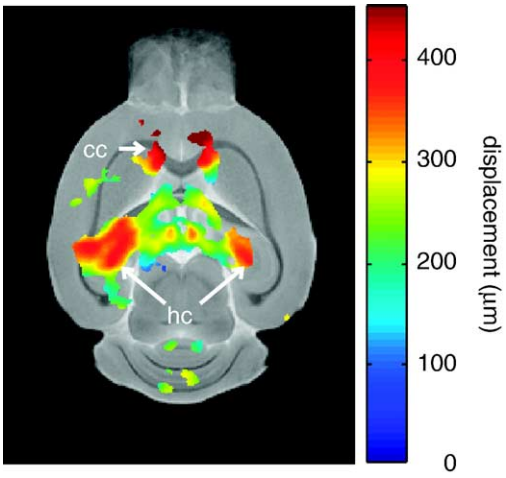

Fig. 5. A representative horizontal view showing statistically significant displacements of the C57 strain in relation to the 129Sv. The color scale corresponds to shifts in micrometers. Parts of the hippocampus (hc) and the corpus callosum (cc) in the C57 show large displacements with respect to the 129Sv (voxels in yellow and red). The blue areas indicate smaller but statistically significant shifts between the two strains, e.g., the anterodorsal thalamus (vertical arrow).

Discussion

The techniques we have developed utilizing MRI and image processing show the feasibility of quickly analyzing 3D structural features in the CNS in a non-destructive manner. We believe that the quantitative determination of variation for sample populations within a strain is necessary before analyzing genetic mutants. In fact, the structural variations we observed between 129Sv and C57 inbred populations highlight the importance of gene expression in influencing CNS morphology. We make note of several features observed in Table 1.

The volumes of a number of structures were found to be quite similar across these three diverse strains. These include the axon tracts of the anterior and posterior commissure, the fimbria, fornix, stria terminalis, and the optic tract. However, several structures showed interesting differences. For example, the C57 mice showed consistently larger total brain volumes compared to the age-matched CD1 mice, despite their substantially smaller gross body weight (23.6 ± 1.2 g versus 31.1 ± 0.9 g). The largest contributors to the increased brain mass in C57 mice were the cerebral cortex and ventricular compartments (lateral and 3rd and 4th ventricles), with increases of 10% and 13% compared to CD1, respectively. The increase in cortical volume seen in C57 mice compared to mice of the CD1 and 129Sv lineages could potentially be related to the improved performance of this strain over the other strains as previous demonstrated in behavioral, learning and memory and sensory tests (Rogers et al., 1999; Crawley, 2000).

An MRI-based volumetric measurement is useful in screening defined populations of mice for the presence of significant morphologic differences. However, caution must be exhibited in equating changes in morphometric parameter to changes in function. For example, 129Sv mice showed increased cerebellar volume (arbor vita and cerebellum gray matter, Table 1) and a nominal increase in hippocampal volume (dentate gyrus and hippocampal gray matter, Table 1) compared to C57 and CD1 mice. However, no experimental studies to date suggest that these animals exhibit improved performance in behaviors tied to either of these structures. We did observe that 129Sv mice have a small but significant reduction in the volume of their corpus callosum compared to the other two strains, consistent with previous reports (Crawley, 2000).

Another benefit of these techniques is that we can accurately characterize entire CNS structures such as the whole striatum, hippocampus, and anterior commissure, which are typically too large to study using histology. We observed that the volume of the striatum differed by approximately 4% between each of the lines in the order CD1 > C57 > 129Sv. Such considerations may be important in choosing the most appropriate strain for studies aimed at depleting a specific target population of vulnerable neurons. The utility of an MRI-based approach to examine structural mutants depends significantly on the chosen control population. We expect that a very stable neural structure in terms of volume will be best suited for studies in which the control and target populations differ only by a single gene product; changes in volume should then be due only to this genetic manipulation. In the present strain comparison, we are making observations on features that represent the interaction of multiple genetic elements.

The volumetric analysis above reduces each measured CNS structure down to one number: its volume. While making comparisons easy, it will miss changes in position relative to surrounding structures and subtle shape changes. For example, we can see that the cortex appears more 'triangular' (viewed horizontally) in the C57 but more square in the other two strains (Fig. 1). It should be possible in future work to precisely define these differences by using more sophisticated techniques using adaptive shape models (Bookstein, 1996), statistical shape models (Rueckert et al., 2003), or space-scale representations (Petrovic et al., 2004) to describe the three-dimensional structures.

We also demonstrated techniques to measure inter-strain differences without the need for labeled anatomy. For example, simple visual inspection in Fig. 2 can be used to convey whether or not a genetic mutant is different from a control sample population. More quantitative information can be found in the deformation fields.

As the deformation field is independent from the labeling information, calculated measurements derived from deformation fields will highlight differences beyond the extent of known structures. For example, the Jacobian will identify regions of volume change that extend outside or are smaller than the known boundaries of a given brain structure (Fig. 4). In the same way, the displacement data show positional shifts in regions of the brain not necessarily tied to known anatomical features. Such powerful methods will allow biologists to study anatomy on a whole-brain scale, similar to recent studies in the human brain (Shen and Davatzikos, 2003; Shen et al., 2002). Combined with the potential high throughput of the imaging and the image analysis, we believe we have a powerful technique for the morphometric analysis of mouse models of human disease.

In conclusion, we have demonstrated several novel and sensitive metrics to compare 3D brain anatomy in a group-wise fashion. We have shown that the intra-strain anatomical differences are significantly smaller than inter-strain differences. We have explored the natural variation within genetically identical strains of mice at a resolution of 60 μm isotropic and found that there are variations in size on the order of 2–15% for different CNS structures within a strain. A number of ways to make group-wise comparisons were demonstrated to show quantitative differences between the strains. We believe that our tools are an important complement to the study of behavioral and physiological differences in strains of inbred mice and will be crucial for finding anatomical mutants.

Acknowledgments

The authors acknowledge the technical support from Nir Lifshitz, Lori Davidson, and Erin Chan. The authors also thank Drs. David Deerfield, Arthur Wetzel, and Stuart Pomerantz for designing the web browser for the brain atlases. The research is funded by the Canada Foundation for Innovation, the Ontario Innovation Trust, the Ontario Research and Development Challenge Fund, the Canadian Institutes of Health Research, and the Burroughs Wellcome Fund.

References

Bookstein, F.L., 1996. Biometrics, biomathematics and the morphometric synthesis. Bull. Math. Biol. 58, 313–365.

Chung, M.K., Worsley, K.J., Paus, T., Cherif, C., Collins, D.L., Giedd, J.N., Rapoport, J.L., Evans, A.C., 2001. A unified statistical approach to deformation-based morphometry. Neuroimage 14, 595–606.

Crawley, J.N., 2000. What's wrong with my mouse? Behavioral Phenotyping of Transgenic and Knockout Mice. Wiley-Liss, New York.

Friston, K.J., Holmes, A., Poline, J.B., Price, C.J., Firth, C.D., 1996. Detecting activations in PET and fMRI: levels of inference and power. Neuroimage 4 (3, Part 1), 223–235.

Idziak, S., Haeberlen, U., 1982. Design and construction of a high homogeneity rf coil for solid-state multiple-pulse NMR. J. Magn. Reson. 50, 281–288.

Kovacevic, N., Chen, J., Sled, J.G., Henderson, J., Henkelman, M., 2004. Deformation based representation of groupwise average and variability. Lect. Notes Comput. Sci. 3216, 616–622.

Kovacevic, N., Henderson, J.T., Chan, E., Lifshitz, N., Bishop, J., Evans, A.C., Henkelman, R.M., Chen, X.J., 2005. A three-dimensional MRI atlas of the mouse brain with estimates of the average and variability. Cereb. Cortex 15, 639–645.

Lancaster, J.L., Kochunov, P.V., Thompson, P.M., Toga, A.W., Fox, P.T., 2003. Asymmetry of the brain surface from deformation field analysis. Hum. Brain Mapp. 19, 79–89.

McIntosh, A.R., Lobaugh, N.J., 2004. Partial least squares analysis of neuroimaging data: applications and advances. Neuroimage 23 (Suppl. 1), S250–S263.

Petrovic, A., Escoda, O.D., Vandergheynst, P., 2004. Multiresolution segmentation of natural images: from linear to nonlinear scale-space representations. IEEE Trans. Image Process. 13, 1104–1114.

Robbins, S., Evans, A.C., Collins, D.L., Whitesides, S., 2004. Tuning and comparing spatial normalization methods. Med. Image Anal. 8, 311–323.

Rogers, D.C., Jones, D.N., Nelson, P.R., Jones, C.M., Quilter, C.A., Robinson, T.L., Hagan, J.J., 1999. Use of SHIRPA and discriminant analysis to characterise marked differences in the behavioural phenotype of six inbred mouse strains. Behav. Brain Res. 105, 207–217.

Rueckert, D., Frangi, A.F., Schnable, J.A., 2003. Automatic construction of 3-D statistical deformation models of the brain using nonrigid registration. IEEE Trans. Med. Imag. 22, 1014–1025.

Shen, D., Davatzikos, C., 2003. Very high-resolution morphometry using mass-preserving deformations and HAMMER elastic registration. Neuroimage 18, 28–41.

Shen, D., Moffat, S., Resnick, S.M., Davatzikos, C., 2002. Measuring size and shape of the hippocampus in MR images using a deformable shape model. Neuroimage 15, 422–434.

Tabibnia, G., Cooke, B.M., Breedlove, S.M., 1999. Sex difference and laterality in the volume of mouse dentate gyrus granule cell layer. Brain Res. 827, 41–45.

Tyszka, J.M., Readhead, C., Bearer, E.L., Pautler, R.G., Jacobs, R.E., submitted for publication. Statistical diffusion tensor histology reveals regional dysmyelination effects in the shiverer mouse mutant. Neuroimage.

Wahlsten, D., Metten, P., Crabbe, J.C., 2003. Survey of 21 inbred mouse strains in two laboratories reveals that BTBR T/+ tf/tf has severely reduced hippocampal commissure and absent corpus callosum. Brain Res. 971, 47–54.

Worsley, K.J., Taylor, J.E., Tomaiuolo, F., Lerch, J., 2004. Unified univariate and multivariate random field theory. Neuroimage 23 (Suppl. 1), S189–S195.